Evidence of surface interlayer dimerization in the commensurate charge density wave phase of 1T-$TaSe_2$

Niccolò Mignani,[1] Alberto Crepaldi,[1,2] Luca Moreschini,[3,4,*] Aaron Bostwick,[5] Chris Jozwiak,[5] Eli Rotenberg,[5] Simon Crampin,[6] Enrico Da Como,[6] and Ettore Carpene[2,†]

[1]*Dipartimento di Fisica, Politecnico di Milano, piazza Leonardo da Vinci 32, 20133 Milano, Italy*
[2]*CNR-IFN, Institute for Photonics and Nanotechnologies, piazza Leonardo da Vinci 32, 20133 Milano, Italy*
[3]*Department of Physics, University of California, Berkeley, California 94720, USA*
[4]*Materials Sciences Division, Lawrence Berkeley National Laboratory, Berkeley, California 94720, USA*
[5]*Advanced Light Source, Lawrence Berkeley National Laboratory, Berkeley, California 94720, USA*
[6]*Department of Physics, Condensed Matter and Quantum Materials group, University of Bath, Claverton Down, Bath, BA2 7AY, United Kingdom*

Van der Waals layered materials offer unprecedented opportunities to tune electronic properties by controlling, for instance, the number of layers or their mutual twist angle. However, the translational degree of freedom has not been given proportionate attention. Within the wide family of transition metal dichalcogenides, the commensurate charge density wave (CCDW) phase of 1T-$TaSe_2$ is predicted to host several quantum states ranging from 1D metal to 3D insulator depending on the lateral stacking. By means of angle-resolved photoemission spectroscopy with micrometer spatial resolution, we studied the charge-ordered 1T-$TaSe_2$, revealing the co-existence of metallic and insulating surface domains. Our investigation clarifies that metallicity is due to a specific lateral sliding of the CCDW layers, while insulating behavior is driven by surface interlayer dimerization. These results open intriguing potentialities in surface functionalization and control of electronic structure.

The van der Waals bonded structure of layered materials continue to provide unique possibilities to tune electronic properties of multilayer systems by designing the twisting angle between crystallographic axes [1, 2]. Aside from changes in the rotational degrees of freedom, strain and lateral sliding can offer equally interesting avenues for novel phenomenology [3, 4]. In quasi-2D charge density wave (CDW) materials the translational or rotational arrangement of the in-plane charge order is gaining much attention. On one hand it appears to be crucial in order to understand the electronic structure of tantalum based dichalcogenides (TaX_2, X = S, Se), opening an important discussion on the nature of the CDW Mott physics [5–10]. On the other hand it has been recently explored as a method to predict new symmetry-breaking transitions or topological states [11, 12]. 1T-$TaSe_2$ exhibits a well documented CDW with $\sqrt{13}\times\sqrt{13}$ in-plane superlattice rotated by 13.9° with respect to the normal phase lattice [13–15]. It features an incommensurate (ICDW) to commensurate (CCDW) transition at 473 K [16] with metal-like resistivity down to a few Kelvin, in clear antithesis with its sulfide counterpart 1T-TaS_2 displaying three orders of magnitude larger resistivity at cryogenic temperature [17]. While the single commensurate layer of 1T-$TaSe_2$ is believed to host a robust Mott insulating state [18, 19] and to exhibit quantum spin liquid behavior [20], the bulk electronic properties do not seem to call for any Mott physics [8, 9]. This long thought anomaly finds a reconciling explanation in the vertical ordering of the layers, as suggested by recent scanning tunneling microscopy (STM) measurements [21] and systematic ab initio calculations [22] that highlighted the existence of multiple quantum states, from quasi-1D metal to 3D band insulator, depending on the relative slab stacking. In a combined angle-resolved photoemission spectroscopy (ARPES) and STM study, the role of dimensionality along the direction perpendicular to the surface has been discussed, but disregarding stacking geometry effects [23].

In this Letter, by exploiting ARPES with micrometer spatial resolution and density functional theory (DFT) calculations, we reveal the co-existence of metallic and insulating domains in the charge-ordered 1T-$TaSe_2$, which are attributed to distinct, vertical alignments of adjacent commensurate layers. The insulating behavior, in particular, is driven by surface interlayer dimerization enabled by a specific stacking. Considering the comparable energy costs of the different slab arrangements, we argue how these results might open important perspectives on the functional manipulation of surface layers or few-layer samples.

ARPES with a beam diameter of ~ 4 μm was carried out at the MAESTRO beamline of the Advanced Light Source in the $70-150$ eV photon energy range. High quality single crystalline 1T-$TaSe_2$ samples grown by chemical vapour transport were post-cleaved in situ and held at 15 K during measurements. All ab initio DFT calculations were performed with the Quantum Espresso code [24–26]. More details on samples, experimental

*Present address: QuTech and Kavli Institute of Nanoscience, Delft University of Technology, PO Box 5046, 2600 GA Delft, The Netherlands
†Electronic address: ettore.carpene@cnr.it

setup and computations are given in the Supplemental Material (SM), Notes 1-3 [27].

Figs. 1a-b show two representative ARPES spectra of different domains, both measured at 90 eV photon energy. The main difference between them is the presence

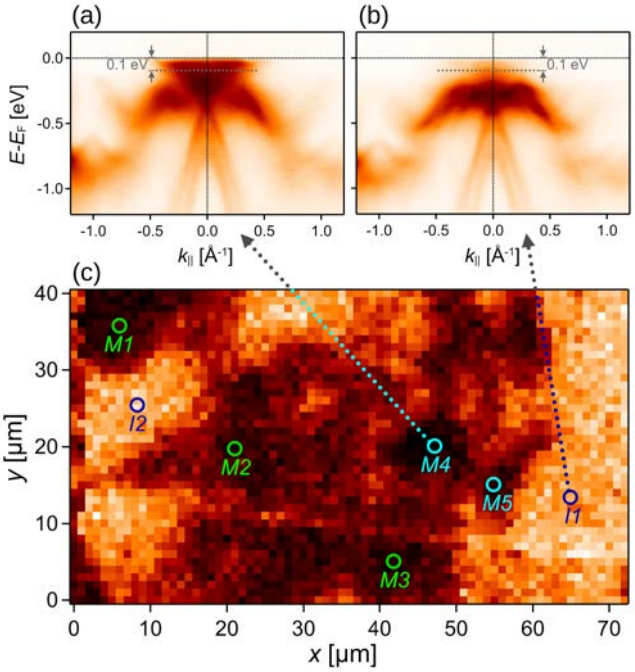

FIG. 1: Two representative ARPES spectra of (a) a metallic domain and (b) an insulating domain measured at 90 eV photon energy. (c) ARPES spatial map (lateral steps of 1 μm): the color contrast is obtained by integrating the photoemission intensity between 0 and 100 meV binding energy. Dark (metallic) domains labelled $M1-M5$ and bright (insulating) domains labelled $I1-I2$ have been investigated in detail.

of the V-shaped metallic state spanning from -0.4 eV at $k_{||}=0$ to the Fermi level in panel 1a, which is not observed in panel 1b. Although a weak spectral signal can be detected at E_F in Fig. 1b, in the following we will refer to these two kinds of domains as metallic and insulating, respectively. By integrating the photoemission intensity between 0 and 100 meV binding energy and mapping the surface over an area of about 70×40 μm^2 with lateral steps of 1 μm, metallic (dark) and insulating (bright) domains with typical size of the order of tens of μm are clearly identified, as shown in Fig. 1c. Several metallic positions, labelled $M1-M5$, and insulating ones, labelled $I1-I2$ have been analyzed in detail (in particular, panel 1a refers to positions $M4$, while panel 1b refers to $I1$), allowing us to group them as $M1-M3$, $M4-M5$ and $I1-I2$ based on their crystallographic orientation, as explained in the following (see also SM, Note 4 [27]).

To understand the physical origin of these domains we first delve into the CCDW structure of 1T-$TaSe_2$. Referring to Fig. 2a, if we label $\mathbf{a_0}$, $\mathbf{b_0}$ and $\mathbf{c_0}$ (the latter is normal to the layer) the three primitive vectors of the undistorted phase, then $\mathbf{a}=3\mathbf{a_0}-\mathbf{b_0}$ and $\mathbf{b}=\mathbf{a_0}+4\mathbf{b_0}$ generate the well known $\sqrt{13}\times\sqrt{13}$ in-plane unit cell of the CCDW phase corresponding to the star-like reconstruction with one Ta atom (labelled A) at the center of each star, 6 nearest neighbours (labelled B) and 6 next nearest neighbours (labelled C) at the tips of the star. Naming $\mathbf{r_i}$ the stacking vectors between two adjacent layers i and $i+1$, the most representative out-of-plane arrangements are shown in Figs. 2b-e. $\mathbf{r_i}=\mathbf{c_0}$ (2b) corresponds to the sequence where all stars are vertically aligned and is described by the space group $P\bar{3}$ (no. 147, in the following we will refer to this stacking as A_s). With $\mathbf{r_i}=\mathbf{a_0}+\mathbf{c_0}$ (2c), each central Ta atom A on layer $i+1$ is aligned to the same nearest neighbours Ta atom B on layer i and is described by the space group $P\bar{1}$ (no. 2, stacking B_s). $\mathbf{r_i}=2\mathbf{a_0}+\mathbf{c_0}$ (2d) corresponds the configuration in which each central Ta atom A on layer $i+1$ is aligned to the same tip Ta atom C on layer i (space group $P\bar{1}$, no. 2, stacking C_s). From the energy viewpoint and in agreement with X-ray and neutron diffraction studies [44–46], the C_s stacking is the most stable configuration since each central Ta atom of a star (where charge density is greatest) on layer i is vertically aligned with a tip of the star (where charge density is least) on layers $i-1$ and $i+1$, minimizing Coulomb repulsion. Due to the trigonal C_3 symmetry of the single slab, the stacking vectors

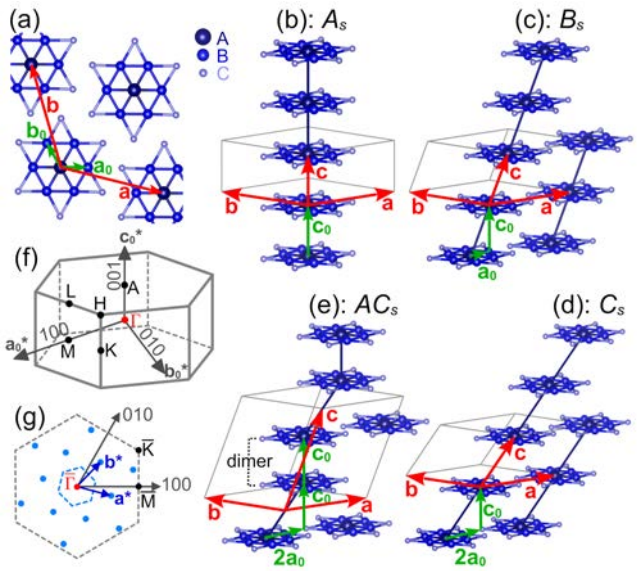

FIG. 2: (a) In-plane lattice reconstruction and primitive vectors of the undistorted ($\mathbf{a_0}$, $\mathbf{b_0}$) and commensurate ($\mathbf{a}$, $\mathbf{b}$) phases (only Ta atoms are shown for clarity). Interlayer stacking: (b) A_s with stacking vector $\mathbf{c_0}$, (c) B_s with stacking vector $\mathbf{a_0}+\mathbf{c_0}$, (d) C_s with stacking vector $2\mathbf{a_0}+\mathbf{c_0}$ and (e) dimerized AC_s with stacking vectors alternating between $2\mathbf{a_0}+\mathbf{c_0}$ and $\mathbf{c_0}$. (f) BZ of the undistorted cell with the most relevant high symmetry points and crystal directions. (g) Surface-projected BZs of undistorted (gray) and commensurate (cyan) cells. Cyan dots are the $\bar{\Gamma}$ points in the commensurate phase.

$2\mathbf{b_0} + \mathbf{c_0}$ and $-2(\mathbf{a_0} + \mathbf{b_0}) + \mathbf{c_0}$ (their in-plane projections are 120° apart) are equally allowed and domains with all three orientations can coexist [46]. Wang et al. [22] considered several inequivalent single- and multilayer sliding stacking sequences, identifying the paired bilayer structure (2e, space group $P\bar{1}$, no. 2, named AC_s hereafter) as the second energetically most favourable after the C_s, a configuration extensively discussed for the related CDW material 1T-TaS_2 [5, 47–52]. In the AC_s stacking, lateral sliding occurs every two slabs and the A_s-like bilayer yields a band insulator phase: each CDW cluster of 13 Ta atoms separately provides one unpaired $5d_{z^2}$ electron and the two $5d_{z^2}$ electrons of the A_s-like dimer form bonding-antibonding states that open a hybridization gap. Although bulk interlayer dimerization is well established in the CCDW phase of 1T-TaS_2, it has never been observed in 1T-$TaSe_2$. In the following, we will provide evidence of its formation at the surface. It should be emphasized that the energy difference between the various stacking configurations is small (a few meV per Ta atom), due to the weak interlayer van der Waals interaction.

Fig. 2f illustrates the first Brillouin zone (BZ) of the undistorted 1T-$TaSe_2$ structure (space group $P\bar{3}m1$, no. 164) with the most significant high symmetry points. Throughout the Letter we will refer to this BZ to identify crystallographic orientations. Fig. 2g shows the surface-projected BZ (gray hexagon), the in-plane basis vectors ($\mathbf{a}^*$ and $\mathbf{b}^*$) of the CCDW phase, its surface-projected BZ (cyan hexagon) and the corresponding centres $\bar{\Gamma}$ (cyan dots) within the undistorted BZ. These features are common to all stacking configurations, which only differ by a commensurate lateral sliding of identical slabs with no twisting angle between adjacent layers (see SM, Note 5 [27]).

We will now illustrate our main experimental and computational results. Fig. 3a shows the Fermi surface (FS) measured at position $M1$ with $h\nu = 90$ eV photon energy (identical features are observed at $M2$ and $M3$, see SM, Note 4 [27]). The shape outlined by the high spectral weight (dark color) clearly lacks C_3 symmetry, ruling out the trigonal $P\bar{3}$ structure A_s. As clarified further below, $h\nu = 90$ eV corresponds to an out-of-plane momentum k_z located about 0.135 (in relative reciprocal lattice units, r.l.u.) above Γ. Panel 3b reports the calculated FS of the C_s stacking at $k_z = 0.135$ r.l.u. unfolded onto the undistorted BZ, exhibiting an excellent agreement with the measurement and allowing us to identify the k_x momentum axis as the $[0\bar{1}0]$ crystallographic direction. Panel 3c shows the FS measured at position $M4$ (essentially identical to $M5$). A close inspection reveals that it is very similar to the FS in panel 3a, but simply rotated clockwise by 120°: thus, by comparing with the computed FS in panel 3d, the k_x momentum axis is assigned to the [100] crystallographic direction.

A further evidence of the C_s interlayer stacking leading to metallic behaviour is obtained exploring the out-of-plane momentum $k_\perp = k_{001}$. Photon energy scans

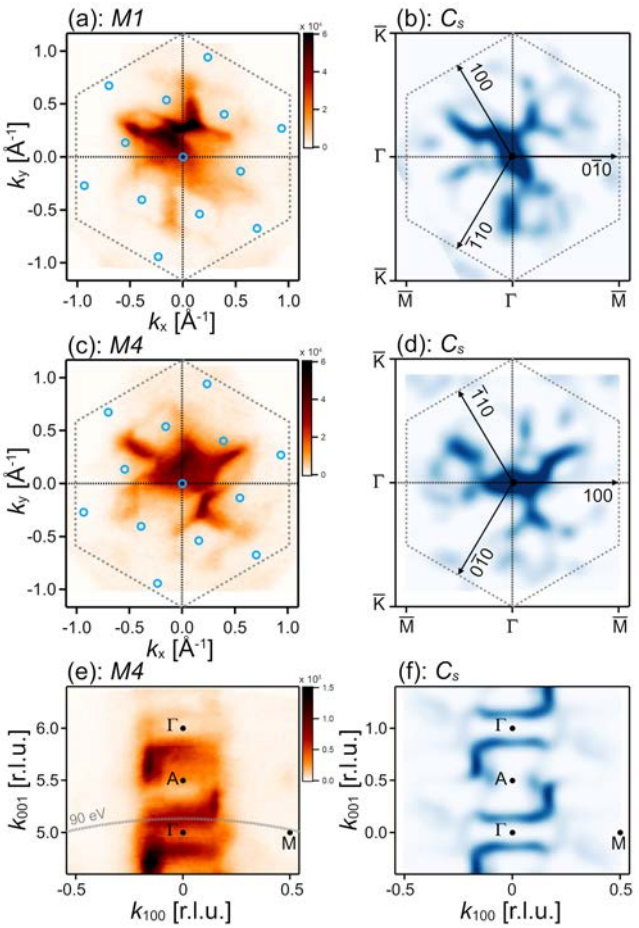

FIG. 3: (a) In-plane FS of domain $M1$ (see Fig. 1c) measured at $h\nu = 90$ eV. The dashed hexagon is the surface-projected BZ of the undistorted lattice, cyan circles mark the $\bar{\Gamma}$ points of the commensurate phase. (b) Calculated FS of the C_s stacking. (c) FS of the metallic domain $M4$. (d) Calculated FS of the C_s stacking (same as panel 3b, but rotated 120° clockwise). (e) Out-of-plane FS of domain $M4$; based on panel (d), the in-plane momentum is k_{100}, the out-of-plane momentum k_{001} results from photon energy scan in the $70-150$ eV range (momenta in r.l.u.). (f) Calculated out-of-plane FS of the C_s stacking in the (k_{100},k_{001}) plane. Relevant dimensions in $Å^{-1}$ are ΓM = 1.04, ΓK = 1.2 and ΓA = 0.5.

in the range $70 - 150$ eV allowed us to cover the entire (undistorted) BZ normal to the layers. With an estimated inner potential $V_0 = 14.5$ eV, the photon energy is converted into $k_\perp$ momentum and the FS on the ($k_{||}$, $k_\perp$) plane is accessed. Panel 3e refers to the metallic domain $M4$, where the in-plane direction is the [100] crystallographic axis (k_x in Fig. 3c). The FS is characterized by broad horizontal nearly straight sections that bend upward/downward when moving along [100]/[$\bar{1}$00] directions, with Γ and A being centrosymmetric points. These features are fully reproduced by the calculated FS of the C_s stacking, unfolded on the undistorted BZ, shown in panel 3f. The gray dotted parabolic line in Fig. 3e represents the 90 eV photon energy contribution to the out-of-

plane FS, the same energy used to acquire the in-plane FS in panels 3a and 3c. In the vicinity of $k_{100} \sim 0$, it corresponds to $k_{001} \sim 0.135$ r.l.u., as stated above. The experimental evidence outlined so far proves that the metallic behavior of $1T$-$TaSe_2$ in the CCDW phase is determined by domains with C_s interlayer stacking and three-fold symmetric relative orientations, in agreement with previous studies [23, 44–46].

The structural origin of the insulating domains is more subtle. Figs. 4a and 4b show the in-plane and out-of-plane FS, respectively, at position $I1$ (equivalent features are observed at $I2$), plotted with the same intensity scale used for the metallic positions (Fig. 3). This allows to assess the strong suppression of spectral weight at the Fermi level in the insulating domains. Enhancing the

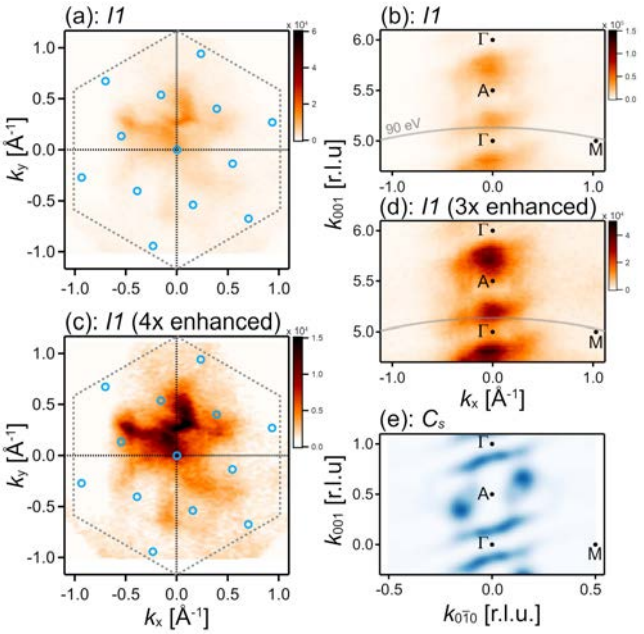

FIG. 4: (a) In-plane FS of domain $I1$ (see Fig. 1c) measured at $h\nu = 90$ eV and shown with the same intensity scale of Figs. 3a and 3c. (b) Out-of-plane FS of domain $I1$ (same intensity of scale of Fig. 3e). (c) As panel (a), with 4× enhanced intensity. Notice the similarities with Fig. 3a, according to which k_x is assigned to the $k_{0\bar{1}0}$ direction. (d) As panel (b), with 3× enhanced intensity. (e) Calculated out-of-plane FS of the C_s stacking and in the ($k_{0\bar{1}0}$,k_{001}) plane.

intensity by a factor of 3 or 4, as shown in Figs. 4c-d, clear patterns emerge. Notice in particular the close resemblance of the in-plane FS (panel 4c) with the one observed at position $M1$ (Fig. 3a). Accordingly, the horizontal momentum axis of the $I1-I2$ domains is assigned to the $[0\bar{1}0]$ crystallographic direction. The out-of-plane FS (Fig. 4d) is characterized by elongated sections centered between the high symmetry points Γ and A of the BZ with a mild positive slope pointing from lower-left to upper-right direction. These features are well replicated by the computed FS of the C_s stacking in the same crystallographic plane, as shown in Fig. 4e (the high spectral weight regions beside the A points can be largely suppress employing the DFT+U computational approach, obtaining a better qualitative agreement with the experimental data without altering our conclusions, see SM Note 6 [27]). Therefore, Fig. 4 delineates a clear scenario for the stacking structure of the insulating domains: they are C_s-like in the bulk, but the strong suppression of spectral weight at the Fermi level indicates the presence of an insulating surface termination. In this circumstance, there can be the possibility of weakly k_{001}-dispersing features in the ARPES spectra, due to electronic states associated with the distinct surface slab. Our analysis indeed confirms the presence of such states.

Fig. 5a tracks the momentum distribution curves (MDCs) at $E - E_F = -0.5$ eV as a function of the out-of-plane momentum k_{001}, spanning the entire BZ. The spectral "shoulders" highlighted by the black arrows and visible over the whole k_{001} range identify the dispersionless features of the surface band (additional proof is given in the SM, Note 7 [27]). The choice of this energy is made such that dispersive and non-dispersive components are clearly distinguishable since they do not overlap for specific ranges of the out-of-plane momentum. This is distinctly revealed in panels 5b-c showing the ARPES spectra at $k_{001} = 5.75$ and 5.25 r.l.u., respectively. Black arrows mark the discernible feature not dispersing along k_{001}. In order to emphasize it, we performed the numerical second derivative of the ARPES data with respect to the energy axis, averaged over the entire BZ in the out-of-plane direction (i.e. $5 \leq k_{001} \leq 6$ r.l.u.), as shown in Fig. 5d. This method enhances localized components since the k_{001}-dependent spectral features are smeared out by the averaging, resulting in negligible second derivative contributions. The band emerging in Fig. 5d has the typical shape given by Ta-5d orbitals in the CCDW phase [8] with a minimum binding energy of ~ 0.2 eV, indicated by gray arrows. The exact same analysis performed on the ARPES spectra of the metallic domain $M4$, shown in Figs. 5e-h, reveals no localized bands in the same energy range. The dispersionless feature at E_F in panel 5h is an artifact due to the abrupt change of spectral weight caused by the Fermi-Dirac distribution.

Hence, by combining the experimental evidence shown in Figs. 4 and 5, we conclude that the structure of the $I1 - I2$ domains is metallic, C_s-like in the bulk, with an insulating termination at the surface. Since our ARPES analysis does not indicate any loss of commensuration in the insulating domain (see also SM, Note 4 [27]), its surface termination is in the CCDW phase as well, but it must deviate from the C_s-like bulk underneath (otherwise metallic behavior would be observed at the surface). In other words, the surface slab in the $I1 - I2$ domains must form either an A_s or a B_s sequence with the underlying neighboring layer. Previous DFT calculations of bulk A_s, B_s and C_s stacking configurations [22] have revealed a common feature along the Γ−A direction normal to the layers: a band ascribed to Ta-

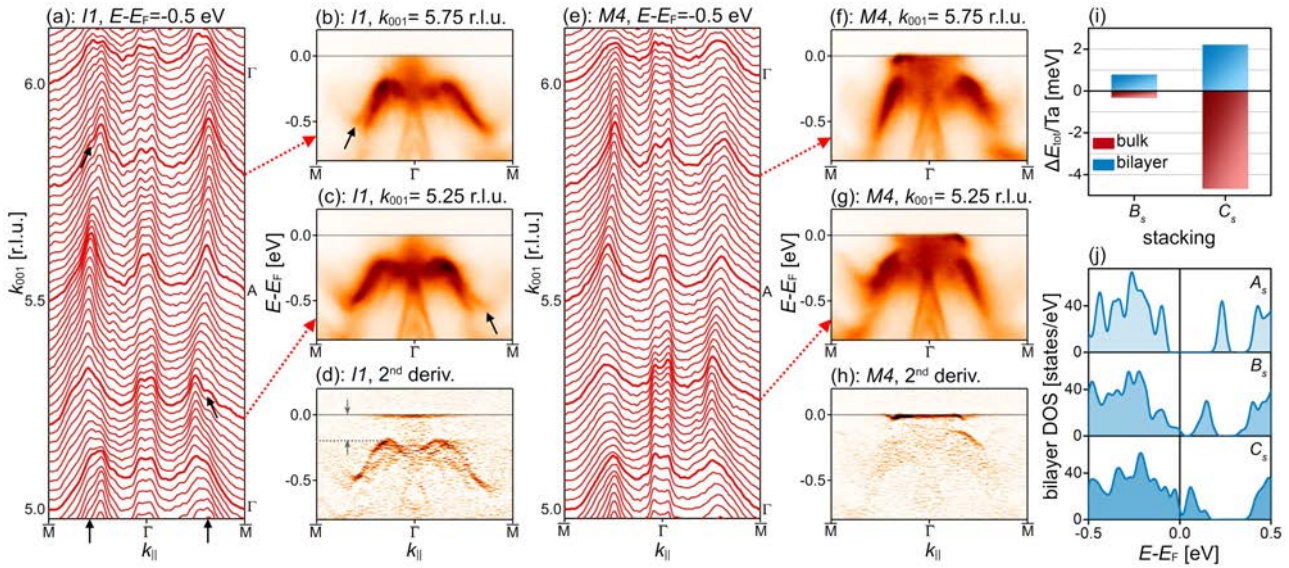

FIG. 5: (a) k_{001}-resolved MDCs of domain $I1$ at $E - E_F = -0.5$ eV: bold lines correspond to $k_{001} = 5, 5.25, 5.5, 5.75$ and 6 r.l.u. (b) ARPES spectra of the insulating domain $I1$ for out-of-plane momentum $k_{001} = 5.75$ and (c) 5.25 r.l.u. Black arrows in panels (a)-(c) highlight the non-dispersive spectral feature of the surface band. (d) Numerical second derivative of the ARPES spectra with respect to the energy axis, averaged over the BZ in the out-of-plane direction ($5 < k_{001} < 6$ r.l.u.), revealing the surface band. (e)-(h) Same as (a)-(d) for the metallic domain $M4$: no surface band is observed. (i) Calculated total energy per Ta atom of bulk (red) and isolated bilayers (blue) in the B_s and C_s stackings (energies relative to the respective A_s configurations). (j) DOS of the three bilayer stackings.

$5d_{z^2}$ orbitals crossing the Fermi level, thus leading to 1D out-of-plane metallicity. Only the C_s-like stacking displays in-plane bands crossing the Fermi level, signal of 3D metallic character. The situation changes in the extreme thin slabs. We performed additional DFT calculations of isolated A_s, B_s and C_s bilayers (see SM, Note 3 [27] for details), yielding relative values of the total energy (ΔE_{tot}) and DOS shown in Figs. 5i-j. While the C_s stacking is the bulk ground state, the A_s stacking is energetically the most favorable bilayer configuration (panel 5i), exhibiting a clear energy gap across the Fermi level (panel 5j). The loss of metallicity in the A_s bilayer is a consequence of the unpaired Ta-$5d_{z^2}$ electrons forming the bonding/antibonding states at the origin of interlayer dimerization. A similar effect is observed in the alternating AC_s stacking sequence (see Fig. 2e) where dimerization involves the A_s bilayers, resulting in a strong reduction of DOS at the Fermi level [22]. Thus, our analysis, in concert with previous computation, clearly indicates that the formation of individual A_s slabs, either within a bulk or at the surface, hinders the metallic behavior through interlayer dimerization. However, in contrast with the related CDW material 1T-TaS_2, where AC_s-like dimers have been observed throughout the bulk, in 1T-$TaSe_2$ the AC_s sequence is limited solely to the surface termination (a comparison among experimental data, C_s and AC_s stacking calculations is reported in the SM Note 3 [27]).

In conclusion, the puzzling coexistence of metallic and insulating domains found here by micro-ARPES in the charged-ordered phase of 1T-$TaSe_2$ finds an unitary explanation in the vertical stacking of the commensurate slabs. While the bulk metallic properties are fully described by the C_s layer sequence (Fig. 2d), that is the ground state of 1T-$TaSe_2$, insulating behaviour occurs at the surface via interlayer dimerization with an A_s-like termination of the metallic domains. If on one hand the formation of bonding/antibonding states in the dimerized layers should lower the surface energy, on the other hand the larger stability of the C_s stacking might compete with dimerization, explaining the absence of a homogeneous insulating surface layer (Fig. 1c). Given the small energy difference between the various stackings (a few tens of meV/star cluster, according to Fig. 5g), thermally activated and reversible switching of metal/insulator character at the surface could provide an alternative scenario to the claimed Mott-like transition [14, 15], opening novel and fascinating perspective on functionalized surfaces or 2D heterostructure devices that will be subject of future investigations.

Note: during the preparation of this work we have become aware of a similar study by Straub *et al.* [53] who also identify two separate terminations with insulating/conductive nature on the 1T-$TaSe_2$ surface.

Acknowledgments: we acknowledge financial supports from the program "Next Generation EU" - PNRR - M4C2, investment 1.1 - Fondo PRIN 2022 - under project CRESO, Grant ID 20223X5Z5E, CUP D53D23002110001 and from PRIN 2020 Quantum Transition-metal FLUOrides (QT-FLUO) - ID

20207ZXT4Z - CUP D43C22000360006. EDC acknowledges support from grant UKRI597: New two dimensional material platforms for nanoscale quantum sensing.

[1] E. Y. Andrei, D. K. Efetov, P. Jarillo-Herrero, A. H. MacDonald, K. F. Mak, T. Senthil, E. Tutuc, A. Yazdani, A. F. Young, Nature Reviews Materials **6**, 201-206 (2021).

[2] Q. Lin, H. Fang, A. Kalaboukhov, Y. Liu, Y. Zhang, M. Fischer, J. Li, J. Hagel, S. Brem, E. Malic, N. Stenger, Z. Sun, M. Wubs, S. Xiao, Nature Comm. **15**, 8762 (2024).

[3] J. S. Alden, A. W. Tsen, P. Y. Huang, R. Hovden, L. Brown, J. Park, D. A. Muller, P. L. McEuen, PNAS **110**, 1125611260 (2013).

[4] F. Escudero, A. Sinner, Z. Zhan, P. A. Pantaleon, F. Guinea, Phys. Rev. Res. **6**, 023203 (2024).

[5] T. Ritschel, H. Berger, J. Geck, Phys. Rev. B **98**, 195134 (2018).

[6] T. Ritschel, J. Trinckauf, K. Koepernik, B. Büchner, M. v. Zimmermann, H. Berger, Y. I. Joe, P. Abbamonte, J. Geck, Nature Phys. **11**, 328-331 (2015).

[7] D. Shin, N. Tancogne-Dejean, J. Zhang, M. S. Okyay, A. Rubio, N. Park, Phys. Rev. Lett. **126**, 196406 (2021).

[8] C. J. Sayers, G. Cerullo, Y. Zhang, C. E. Sanders, R. T. Chapman, A. S. Wyatt, G. Chatterjee, E. Springate, D. Wolverson, E. Da Como, E. Carpene, Phys. Rev. Lett. **130**, 156401 (2023).

[9] C. J. Sayers, Y. Zhang, C. E. Sanders, R. T. Chapman, A. S. Wyatt, G. Chatterjee, E. Springate, G. Cerullo, D. Wolverson, E. Da Como, E. Carpene, Commun. Phys. **7**, 389 (2024).

[10] C. J. Sayers, H. Hedayat, A. Ceraso, F. Museur, M. Cattelan, L. S. Hart, L. S. Farrar, S. Dal Conte, G. Cerullo, C. Dallera, E. Da Como, E. Carpene, Phys. Rev. B **102**, 161105 (2020).

[11] F. Cossu, D. Nafday, K. Palotás, M. Biderang, H.-S. Kim, A. Akbari, I. Di Marco, Phys. Rev. Res. **6**, 043111 (2024).

[12] J. M. Pizarro, S. Adler, K. Zantout, T. Mertz, P. Barone, R. Valentí, G. Sangiovanni, T. O. Wehling, npj Quantum Materials **5**, 79 (2020).

[13] M. Bovet, D. Popović, F. Clerc, C. Koitzsch, U. Probst, E. Bucher, H. Berger, D. Naumović, P. Aebi, Phys. Rev. B **69**, 125117 (2004).

[14] L. Perfetti, A. Georges, S. Florens, S. Biermann, S. Mitrovic, H. Berger, Y. Tomm, H. Höchst, M. Grioni, Phys. Rev. Lett. **90**, 166401 (2003).

[15] S. Colonna, F. Ronci, A. Cricenti, L. Perfetti, H. Berger, M. Grioni, Phys. Rev. Lett. **94**, 036405 (2005).

[16] J. A. Wilson, F. J. Di Salvo, S. Mahajan, Phys. Rev. Lett. **32**, 882-885 (1974).

[17] J.A. Wilson, F.J. Di Salvo, S. Mahajan, Adv. Phys. **24**, 117-201 (1975).

[18] Y. Chen, W. Ruan, M. Wu, S. Tang, H. Ryu, H.-Z. Tsai, R. L. Lee, S. Kahn, F. Liou, C. Jia, O. R. Albertini, H. Xiong, T. Jia, Z. Liu, J. A. Sobota, A. Y. Liu, J. E. Moore, Z.-X. Shen, S. G. Louie, S.-K. Mo, M. F. Crommie, Nat. Phys. **16**, 218 (2020).

[19] Y. Nakata, K. Sugawara, A. Chainani, H. Oka, C. Bao, S. Zhou, P.-Y. Chuang, C.-M. Cheng, T. Kawakami, Y. Saruta, T. Fukumura, S. Zhou, T. Takahashi, T. Sato, Nat. Commun. **12**, 5973 (2021).

[20] W. Ruan, Y. Chen, S. Tang, J. Hwang, H.-Z. Tsai, R. L. Lee, M. Wu, H. Ryu, S. Kahn, F. Liou, C. Jia, A. Aikawa, C. Hwang, F. Wang, Y. Choi, S. G. Louie, P. A. Lee, Z.-X. Shen, S.-K. Mo, M. F. Crommie, Nat. Phys. **17**, 1154 (2021).

[21] W. Zhang, Z. Wu, K. Bu, Y. Fei, Y. Zheng, J. Gao, X. Luo, Z. Liu, Y.-P. Sun, Y. Yin, Phys. Rev. B **105**, 035110 (2022).

[22] W. Wang, B. Zhao, X. Ming, C. Si, Adv. Funct. Mater. **33**, 2214583 (2023).

[23] N. Tian, Z. Huang, B. G. Jang, S. Guo, Y.-J. Yan, J. Gao, Y. Yu, J. Hwang, C. Tang, M. Wang, X. Luo, Y. P. Sun, Z. Liu, D.-L. Feng, X. Chen, S.-K. Mo, M. Kim, Y.-W. Son, D. Shen, W. Ruan, Y. Zhang, National Science Review **11**, nwad144, (2024).

[24] P. Giannozzi *et al.*, J. Phys.: Condens. Matter **21** 395502, (2009).

[25] P. Giannozzi *et al,*, J. Phys.: Condens. Matter **29**, 465901 (2017).

[26] P. Giannozzi *et al.*, J. Chem. Phys. **152**, 154105 (2020).

[27] See Supplemental Material at [url of Supplemental Material] for additional experimental and computational results, which includes Refs. [28–43].

[28] F. J. Di Salvo, R. G. Maines, J. V. Waszczak, and R. E. Schwall, Solid State Commun. **14**, 497 (1974).

[29] R. J. Koch, C. Jozwiak, A. Bostwick, B. Stripe, M. Cordier, Z. Hussain, W. Yun, E. Rotenberg, Synchrotron Radiat. News **31**, 50-52 (2018).

[30] G. Prandini, A. Marrazzo, I. E. Castelli, N. Mounet, E. Passaro, J. Yu, N. Marzari, Materials Cloud Archive **2023.65** (2023).

[31] D. Chakraborty, K. Berland, T. Thonhauser, J. Chem. Theory Comput. **16**, 5893-5911 (2020).

[32] T. Thonhauser, S. Zuluaga, C. A. Arter, K. Berland, E. Schröder, P. Hyldgaard, Phys. Rev. Lett. **115**, 136402 (2015).

[33] T. Thonhauser, V. R. Cooper, S. Li, A. Puzder, P. Hyldgaard, D. C. Langreth, Phys. Rev. B **76**, 125112 (2007).

[34] K. Berland, V. R. Cooper, K. Lee, E. Schröder, T. Thonhauser, P. Hyldgaard, B. I. Lundqvist, Rep. Prog. Phys. **78**, 066501 (2015).

[35] D. C. Langreth et al., J. Phys.: Condens. Matter **21**, 084203 (2009).

[36] P. V. C. Medeiros, S. Stafström, J. Björk, Phys. Rev. B **89**, 041407(R) (2014).

[37] P. V. C. Medeiros, S. S. Tsirkin, S. Stafström, J. Björk, Phys. Rev. B **91**, 041116(R) (2015).

[38] M. Iraola, J. L. Mañes, B. Bradlyn, T. Neupert, M. G. Vergniory, S. S. Tsirkin, Comp. Phys. Commun. **272**, 108226 (2022).

[39] M. B. Walker and R. L. Withers Phys. Rev. B **28**, 2766 (1983).

[40] K. Nakanishi and H. Shiba, J. Phys. Soc. Jpn. **53**, 1103 (1984).

[41] K. Momma and F. Izumi, J. Appl. Crystallogr. **44**, 1272-1276 (2011).

[42] R. Bianco, M. Calandra, F. Mauri, Phys. Rev. B **92**,

094107 (2015).
[43] C. Lian, S.-J. Zhang, S.-Q. Hu, M.-X. Guan, S. Meng, Nat. Commun. **11**, 43 (2020).
[44] D. E. Moncton, F. J. DiSalvo, J. D. Axe, L. J. Sham, B. R. Patton, Phys. Rev. B **14**, 3432 (1976).
[45] R. Brouwer, F. Jellinek, Physica B+C **99**, 51 (1980).
[46] G. A. Wiegers, J. L. de Boer, A. Meetsma, S. van Smaalen, Z. Kristallogr. **216** 45 (2001).
[47] S.-H. Lee, J. S. Goh, D. Cho, Phys. Rev. Lett. **122**, 106404 (2019).
[48] C.-K. Li, X.-P. Yao, J. Liu, G. Chen, Phys. Rev. Lett. **129**, 017202 (2022).
[49] S. L. L. M. Ramos, B. R. Carvalho, R. L. M. Lobato, J. Ribeiro-Soares, C. Fantini, H. B. Ribeiro, L. Molino, R. Plumadore, T. Heinz, A. Luican-Mayer, M. A. Pimenta, ACS Nano **17**, 15883 (2023).
[50] Q. Stahl, M. Kusch, F. Heinsch, G. Garbarino, N. Kretzschmar, K. Hanff, K. Rossnagel, J. Geck, T. Ritschel, Nat. Commun. **11** 1247 (2020).
[51] G. von Witte, T. Kisslinger, J. G. Horstmann, K. Rossnagel, M. A. Schneider, C. Ropers, L. Hammer, Phys. Rev B **100**, 155407 (2019).
[52] J. Dong, D. Shin, E. Pastor, T. Ritschel, L. Cario, Z. Chen, W. Qi, R. Grasset, M. Marsi, A. Taleb-Ibrahimi, N. Park, A. Rubio, L. Perfetti, E. Papalazarou, 2D Mater. **10**, 045001 (2023).
[53] M. Straub, F. Petocchi, C. Witteveen, F. B. Kugler, A. Hunter, Y. Alexanian, G. Gatti, S. Mandloi, C. Polley, G. Carbone, J. Osiecki, F. O. von Rohr, A. Georges, F. Baumberger, A. Tamai, Phys. Rev. Lett. **135**, 096501 (2025).